Communications in Nonlinear Science and Numerical Simulation 110 (2022) 106396

Contents lists available at ScienceDirect

Communications in Nonlinear Science and Numerical Simulation

journal homepage: www.elsevier.com/locate/cnsns

Research paper

Periodic solutions of a tapping mode cantilever in an Atomic Force Microscope with harmonic excitation

Daniel Cortés [a,*], Alexander Gutierrez [a], Johan Duque [b]

[a] *Departamento de Matemáticas-Universidad Tecnológica de Pereira, Carrera 27-10-02 Barrio Alamos, Pereira, 660003, Risaralda, Colombia*
[b] *CIMTE Agrienvironment Engineering-Universidad Tecnológica del Uruguay, Maciel sn/esq Morquio, Durazno, 97000, Durazno, Uruguay*

ARTICLE INFO

Article history:
Received 26 September 2021
Received in revised form 14 February 2022
Accepted 3 March 2022
Available online 15 March 2022

Keywords:
Periodic solution
Cantilever vibrations
Atomic Force Microscope
Lower and upper solutions
Singularities

ABSTRACT

In this paper, we establish the existence and multiplicity for periodic solutions of the nonlinear system associated with a tapping mode cantilever Atomic Force Microscope (AFM) with Lennard-Jones potential and an external harmonic excitation. The technique used to solve the nonlinear system is based in the classical nonlinear technique of lower and upper solutions in reverse order. Finally, we show some numerical simulations using the Poincaré map to present regions where the existence is guaranteed.

1. Introduction

Since the invention of the Atomic Force Microscope (AFM) in 1986 by Quate et al. [1], its applications have been very useful in different fields of science and industry, for example, J. Deng et al. [2], use the AFM as a nano-machine to create nanostructures, C. Hail et al. used the AFM for applications at the quantum level of nano printed organic molecules to create nanophotonic devices [3]. An AFM measures the atomic interactions between particles by allowing the nanoscale study of different nanomaterial surfaces [4,5]. The vibrating tip of an AFM interacts with a surface which makes possible to obtain molecular resolution images of membrane proteins in aqueous solutions or to resolve atomic-scale surface defects in ultra-high vacuum (UHV) [6,7]. Other applications can be found in [8–11]. Recent studies in artificial intelligence found that these computational techniques could be useful for enhancing the AFM analysis and operation, [12–14]. Understanding the mathematical relationship of the parameters in the equation with the real parameters of an AFM allows improving the design and operation of the AFMs, by enhancing the measurement techniques and the resolution of the images. Limitations in AFM design arise in the mathematical modeling of these devices, especially when they present non-linear effects. For example, squeeze film-damping and tip stiffness [7,15].

1.1. Mathematical model of the vibrating tip in an AFM

The AFM cantilever could operate principally in two modes, amplitude modulation atomic force microscopy (AM-AFM), also known as tapping-mode, and frequency modulation atomic force microscopy (FM-AFM), also known as a non-contact

* Corresponding author.
E-mail address: danielcorteszapata@gmail.com (D. Cortés).

https://doi.org/10.1016/j.cnsns.2022.106396
1007-5704/

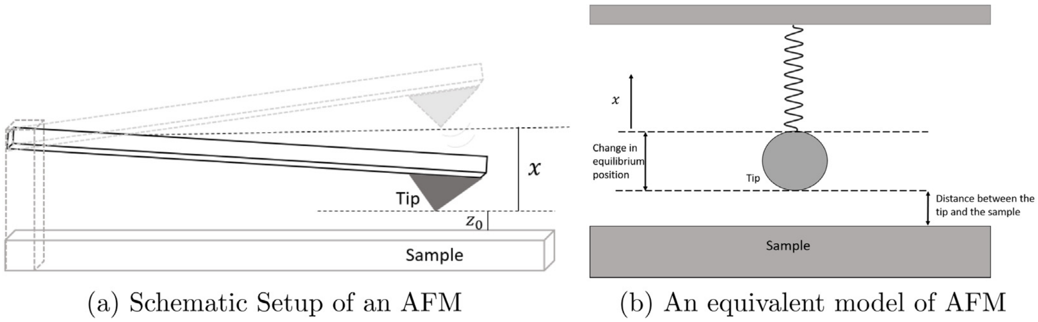

Fig. 1. An equivalent model of AFM, where Z_0 is associated with the distance of the tip from the sample and x determine the movement of the tip.

mode. Fig. 1 shows the schematic setup of an AFM and the interaction between the cantilever beam and the sample. The dynamics of a vibrating tip can be seen as a spring–mass system as illustrated in Fig. 1b. This model is a good approximation to understand the behavior of an AFM in tapping-mode operation [16]. Theoretical analysis of AM-AFM is interesting in many cases due to the coexistence of two stable oscillations states associated to low and high amplitude solutions, due to the presence of the nonlinear tip–sample interaction [6].

In the mathematical model considered here, the beam has an effective mass m and an effective stiffness k. The tip of the cantilever beam is modeled as a sphere of radius R. The cantilever tip is assumed to be placed initially in Z_0, this distance represents the tip–sample separation in the absence of any interaction between them. Additionally, the cantilever has a harmonic external excitation force $h(t)$. The equation of motion governing the displacement of the cantilever tip (vibration) under the influence of the Lennard-Jones force can be written as:

$$mx'' + kx = \frac{A_1 R}{180(Z_0 + x)^8} - \frac{A_2 R}{6(Z_0 + x)^2} + h(t). \tag{1}$$

The first term on the Lennard-Jones force describes a short-range repulsive force due to overlapping electron orbits, called Pauli repulsion, whereas the second term simulates the long-range attraction due to van der Waals forces. This is a special case of the wider family of Mie forces $F_{n,m}(x) = \frac{C}{x^n} - \frac{D}{x^m}$, where n, m are positive integers with $n > m$, also known as the $n - m$ Lennard-Jones force [17,18].

The Eq. (1) is re-scaled according to Ashhab et al. [16] to obtain the dimensionless differential equation

$$y'' = m(y) + f(t) + a, \tag{2}$$

where $m(y) = \frac{1}{y^8} - \frac{b}{y^2} - y$, with $y > 0$ as the vertical displacement of the microcantilever, a, b are positives constants, f is continuous, T-periodic and satisfies

$$\bar{f} = \frac{1}{T}\int_0^T f(s)ds = 0.$$

Some analytical and numerical studies about AFM models under the influence of the Lennard-Jones force can be found in [4,16,19–22]. Despite a large number of related papers, the mathematical understanding of this system is still far from being complete. It can be observed that (2) is an example of an ODE with a singularity at the state variable and periodic dependence on time. Some interesting models with singularities can be found in [15].

1.1.1. Some previous results

In this subsection, we present some previous results associated with the AFM differential Eq. (2). Here below we will denote $\|\cdot\|_\infty$ as the usual supremum norm, $\mathbb{R}^+$ as the set of positive real numbers, $C^n(\mathbb{R}/T\mathbb{Z})$ as the set of functions $u : \mathbb{R} \to \mathbb{R}$, such that $u \in C^n$ and T-periodic, i.e. $u(t + T) = u(t)$.

When $f \equiv 0$, the constant solutions (equilibria) of Eq. (2) are given by the set

$$\mathcal{G} = \{y \in \mathbb{R}^+ : m(y) + a = 0\},$$

whose number of elements, $|\mathcal{G}|$, depends on the parameters a and the critical value of the parameter b

$$b^* = \frac{3}{4^{1/3}}, \tag{3}$$

such that if $b \leq b^*$, Eq. (2) has a unique equilibrium for each a, and if $b > b^*$, (2) can have either one, two or three equilibria, depending on the parameter a, see Fig. 2.

Gutierrez et al. in [23] have studied each of these cases. They have not only established analytically the bifurcation diagram of the equilibria for specific regions of the involved parameters, but also the existence of a couple of saddle–node

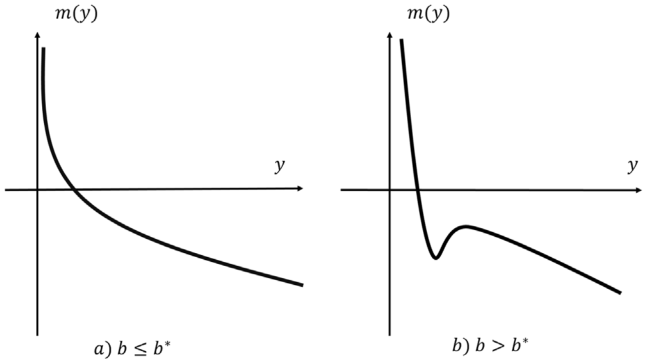

Fig. 2. Two generic cases for the function m. (a) if $b \leq b^*$, $|\mathcal{G}| = 1$. (b) if $b > b^*$, $|\mathcal{G}| = 1, 2$ or 3.

bifurcation. Additionally, in [24], conditions for persistence of the homoclinic orbit were established by Melnikov's method when the model has nonlinear friction and $f \not\equiv 0$. In this sense, the analytical and numerical approaches were presented to verify the solutions of the model, other studies about stability of periodic oscillations can be found in [25,26].

In this paper, we established analytical conditions over the AFM parameter which are necessary for the existence and multiplicity of T-periodic solutions of Eq. (2), by using the lower and upper solutions method in non-well order. In addition, numerical simulations of the dynamical system associated with the model were implemented for verification of the theoretical results. The paper is structured as follows: In Section 2, some previous results about lower and upper solutions method in non-well order are presented, which will be used in the following sections. In Section 3, we present the results related to the existence of at least one T-periodic solution (Theorems 3 to 9). In Section 4, we proof the multiplicity result, Theorems 10 and 11. Finally, in Section 5, numerical examples are studied, showing the existence of a unique periodic solution for suitable conditions on the parameter a and the multiplicity, these numerical examples allow us to establish a method to "trap" those solutions in the estimated region. Finally, we present some numerical examples when the parameter a is changed such that does not satisfy the necessary conditions and the system may present some strange behavior.

2. Materials and methods

2.1. Method of upper and lower solutions

In this section, the notion of upper and lower solutions is used together with some other tools that will let us characterize the stability of periodic solutions in the AFM Eq. (2). The following Lemma allows us to characterize the stability of the solutions for the Hill's equation by means of the characteristic multipliers, this idea can be applied to the AFM equation, see [27].

Lemma 1 (*Lemma 1, [28]*)**.** *Let $w(t)$ be a non-constant continuous T-periodic function such that $w(t) \leq \left(\frac{\pi}{T}\right)^2$ for all t. Then, Hill's equation $y'' + w(t)y = 0$ does not admit negative Floquet multipliers. Moreover, if $w(t) > 0$ for all t, then Hill's equation does not admit real Floquet multipliers.*

This lemma will help us know when the linear problem has an elliptic solution. Remember that a T-periodic solution is elliptic when the linearized equation is elliptic, i.e, the Floquet multipliers are different from ± 1 and have modulus 1. Consequently the linearized equation is stable; however, the stability of the solution cannot be guaranteed due to the dependence of the non-linear terms.

On the other hand, the notion of upper and lower solutions will be used [29]. Given the equation,

$$y'' + g(t, y) = 0, \tag{4}$$

when g is continuous and T-periodic in the first variable, the functions $\alpha, \beta \in C^2(\mathbb{R}/T\mathbb{Z})$ are called lower and upper solutions, respectively, if for all $t \in \mathbb{R}$,

$$\alpha'' + g(t, \alpha) \geq 0$$
$$\beta'' + g(t, \beta) \leq 0.$$

A lower (resp. upper) solution is said to be strict if the above inequality is strict for all $t \in \mathbb{R}$. Let us now assume that α and β are ordered, i.e.,

$$\alpha(t) \leq \beta(t) \quad \text{for all } t \in \mathbb{R}.$$

It is well-known that (4) has a solution lying between α and β, see [29]. However, when α and β are ordered reversely, i.e.,

$$\alpha(t) \geq \beta(t) \quad \text{for all } t \in \mathbb{R},$$

we cannot guarantee the existence of a solution to (4) between β and α. It is necessary to add a suitable non-resonance condition [30].

Proposition 2. *Assume there are upper and lower solutions to (4) such that $\beta(t) < \alpha(t)$ for all t and g is continuously differentiable in the second variable. Under the assumption*

$$g_y(t, y) \leq \left(\frac{\pi}{T}\right)^2 \quad \text{for any } y \in [\beta(t), \alpha(t)], \quad \text{and any } t \tag{5}$$

the equation has a T-periodic solution φ such that $\beta(t) < \varphi(t) < \alpha(t)$.

2.2. Numerical approach

We implemented numerical examples using the Poincaré maps associated with the solutions of the system (2), with algorithms in Python to find those solutions [31]. We set the initial conditions and the parameters b, $\|f\|_\infty$ and T, and we adequately estimated the parameter a such that the established conditions are met. Applying these variations to the distance between the tip and the sample, we could find rich dynamics of the system, establishing numerical criteria for solutions of the system according to the tip–sample distance to study the stability of oscillation of the vibrating tip, where various strange attractors were plotted using Python as shown in Section 4, for certain parameters values and it is in agreement with the theoretical results found in this work, which are shown in the following section.

3. Results and discussion

3.1. Existence of periodic solutions

In this section, we establish the conditions for the existence of periodic solutions in Eq. (2). In order to formulate the main results, let us define the set

$$L = \left\{ y \in \mathbb{R}^+ : m'(y) = -\left(\frac{\pi}{T}\right)^2 \right\}.$$

When $T \leq \pi$, L has a unique solution, independently of the value of b.

In contrast, when $T > \pi$, the number of solutions L depend on b:

(i) When

$$b < b^* \left(1 - \left(\frac{\pi}{T}\right)^2\right),$$

is satisfied, then the set L has no solutions.

(ii) When either $b > b^*$ or

$$(\mathbf{A}) \quad b^* \left(1 - \left(\frac{\pi}{T}\right)^2\right) < b < b^*,$$

occurs, then the set L always has two solutions.

In Fig. 3 region I corresponds to the case when L has one solution ($T \leq \pi$), which will be noted as y_0. Region II shows when L has no solutions, and on regions III and IV L has two solutions that will be denoted as y_1 and y_2.

Now, we present the main results associated with the existence of T-periodic solutions. First we established existence when the function m is decreasing i.e. when $b < b^*$.

For the first theorem we define the interval

$$I_1 =]\|f\|_\infty - m(y_0), \infty[\,,$$

this theorem is related to the lower part of region I, Fig. 3.

Theorem 3. *If $T \leq \pi$ and $b < b^*$, then for each $a \in I_1$ Eq. (2) has at least one elliptic T-periodic solution $\varphi(t)$ such that*

$$r_a < \varphi(t) < R_a.$$

Proof. Note that L has a unique solution, namely y_0. Then, when $a \in I_1$, $m(y_0) > \|f\|_\infty - a$; therefore, $y_0 = r_a$ is an upper solution. On the other hand, we can find the lower solution R_a such that $m(R_a) < -\|f\|_\infty - a$. Moreover, $y_0 < R_a$ and for Proposition 2, there is a T-periodic solution $\varphi(t)$ between y_0 and R_a. Finally, φ is elliptic which follows from Lemma 1 because $0 < w(t) < (\frac{\pi}{T})^2$, where $w(t) = -m'(\varphi(t))$. □

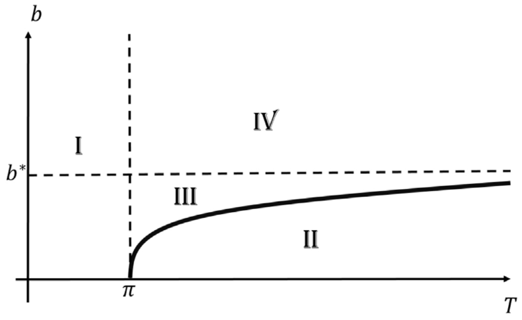

Fig. 3. Diagram for the number of solutions of L in the plane T-vs-b.

Similarly, for $T > \pi$, we define the interval

$$I_2 = \left] \, \|f\|_\infty - m(y_1), -m(y_2) - \|f\|_\infty \, \right[,$$

and we meet the conditions when hypothesis (A) is satisfied, that is on region III, Fig. 3.

Theorem 4. *If $T > \pi$, b satisfies (A) and $\|f\|_\infty < \frac{1}{2}(m(y_1) - m(y_2))$, then for each $a \in I_2$ Eq. (2) has an elliptic T-periodic solution $\varphi(t)$ such that*

$$r_a < \varphi(t) < R_a.$$

Theorem 4 will be demonstrated in the same way as Theorem 3 by the technique of lower and upper solutions.

Proof. Note that L has two points such that $y_1 < y_2$. Because of the hypothesis about the norm of f, we can guarantee that for $a \in I_2$, $m(y_2) < -\|f\|_\infty - a < \|f\|_\infty - a < m(y_1)$ and we take the constant upper solution $\beta = y_1$ and the constant lower solution $\alpha = y_2$. To see that it is elliptic, use the argument used in the proof of Theorem 3. □

Remark 1. If we assume $\|f\|_\infty \geq \frac{1}{2}(m(y_1) - m(y_2))$ in the last theorem, the existence of T-periodic solutions does not lie between the lower and upper solution because it does not fulfill Proposition 2. In this case, it can be shown that the solution is unique by following an argument given in [28].

Finally, the critical case, $b = b^*$, is also studied. In this case, we do not need to restrict the period to guarantee the existence of periodic solutions. To prove Theorem 5, two cases will be studied: when $T \leq \pi$, we use the same argument as in Theorem 3, and when $T > \pi$, we use the argument given in Theorem 4.

Theorem 5. *If $b = b^*$, then there exist a such that (2) has an elliptic T-periodic solution $\varphi(t)$ and*

$$r_a < \varphi(t) < R_a.$$

Proof. If $T \leq \pi$, take the upper and lower solutions $\beta = \left(\frac{4}{b}\right)^{1/6}$ and $\alpha = R_a$ such that $m(R_a) < -\|f\|_\infty - a$, respectively. When $T > \pi$, take $\beta = y_1$ and the constant lower solution $\alpha = y_0$. To see that it is elliptic we use the same argument from Theorem 3. □

Now, we establish conditions for the existence of T-periodic solutions for the case $b > b^*$, region IV in Fig. 3. In this case, the function $m(y)$ has a local minimum in y_l and a maximum in y_r such that $y_l < y_r$. These points correspond to the positive roots of $m'(y)$, where it can be computed as follows:

$$y_l = \left(\frac{4}{3} b \cos\left(\frac{1}{3}\arccos\left(1 - \frac{1}{2}\left(\frac{3}{b}\right)^3\right) + \frac{4}{3}\pi\right) + \frac{2}{3} b\right)^{1/3},$$

$$y_r = \left(\frac{4}{3} b \cos\left(\frac{1}{3}\arccos\left(1 - \frac{1}{2}\left(\frac{3}{b}\right)^3\right)\right) + \frac{2}{3} b\right)^{1/3}.$$

For the following theorems, we denote

$$\hat{y}_r = \min\{y \in \mathbb{R}^+ : m(y) = m(y_r)\}, \qquad \hat{y}_l = \max\{y \in \mathbb{R}^+ : m(y) = m(y_l)\},$$

$$T_r = \frac{\pi}{\sqrt{-m'(\hat{y}_r)}}, \qquad T_l = \frac{\pi}{\sqrt{-m'(\hat{y}_l)}}.$$

These values will help us guarantee the existence of the solution between the non-well ordered pair of lower and upper solutions.

The proofs of Theorems 6 through 9 use the relationship of the period T with the values T_r, T_l and π, which allows us to meet local monotony conditions of m such that the hypothesis of Proposition 2 is satisfied.

For the next two theorems, we define the interval

$$I_3 = \Big] \, \|f\|_\infty - m(y_0), \infty \Big[\, .$$

Theorem 6. *If $b > b^*$ and $T < T_r \leq \pi$ or $T < \pi < T_r$, for each $a \in I_3$, Eq. (2) has at least one T-periodic solution $\varphi(t)$ such that*

$$y_1 < \varphi(t) < R_a.$$

To show Theorem 6, we will consider the set

$$H_a = \{y \in \mathbb{R}^+ : m(y) = -\|f\|_\infty - a\},$$

which is non-empty and compact.

Proof. Note that the set L has a unique solution y_0 if $T < T_r < \pi$ or $T < \pi < T_r$. For these values of T the function m is such that $m(y_0) > m(y_r)$.

Consequently, each $a \in I_3$ satisfies the inequality $\|f\|_\infty - a < m(y_0)$. Then, $r = y_0$ is an upper solution and taking the lower solution such that $R_a > \min H_a$, there is a T-periodic solution between y_0 and R_a. □

Theorem 7. *If $b > b^*$, $T_r < T < \pi$ and $\|f\|_\infty > \dfrac{1}{2} |(m(y_0) - m(y_l))|$, for each $a \in I_3$ Eq. (2) has at least one T-periodic solution.*

Proof. Once again, L has an unique solution y_0 if $T_r < T < \pi$. Consider $T > T_r$, then $m(y_r) > m(y_0)$ so y_r is an upper solution. By the hypothesis about a, $\|f\|_\infty - a < m(y_0)$, and by the hypothesis about the norm of f, $m(y_l) > -\|f\|_\infty - a$. This implies that for each a, the set H_a has a unique solution that satisfies the hypothesis but it suffices to take $R_a > \min H_a$. □

In the same way that in the case $b < b^*$, here we study the cases when $T \leq \pi$ as in the last theorem and the case $T > \pi$, as in the next theorem. Again, we define the interval

$$I_4 = \Big] \, \|f\|_\infty - m(y_1), -m(y_l) - \|f\|_\infty \Big[\, .$$

Theorem 8. *If $b > b^*$, $T_r < \pi < T$ or $\pi < T_r < T$ and $\|f\|_\infty < \dfrac{1}{2} |m(y_1) - m(y_l)|$, for each $a \in I_4$, Eq. (2) has at least one T-periodic solution $\varphi(t)$ such that*

$$y_1 < \varphi(t) < R_a.$$

Proof. If $T_r < \pi < T$ or $\pi < T_r < T$, the set L has two solutions $y_1 < y_2$. By hypothesis, $m(y_l) < -\|f\|_\infty - a < \|f\|_\infty - a < m(y_1)$. Choosing $R_a < y_l$ such that $m(y_l) < m(y) < -\|f\|_\infty - a$, we have proved the assertion. □

Now for the intervals

$$I_5 =]\|f\|_\infty - m(y_l), -m(y_2) - \|f\|_\infty[\, , \; I_6 = \big]\|f\|_\infty - y_1, -\hat{y}_r - \|f\|_\infty\big[\, ,$$

we have the next theorem.

Theorem 9. *If $b > b^*$, $\pi < T < T_l$ and $\|f\|_\infty < \frac{1}{2}(m(y_l) - m(y_2))$ (resp. $\|f\|_\infty < \frac{1}{2}(m(y_1) - m(\hat{y}_r))$), then for each $a \in I_5$ (resp. $a \in I_6$), (2) has at least one T-periodic solution $\varphi(t)$ such that*

$$\hat{y}_l < \varphi(t) < y_2. \quad (\text{ resp. } y_1 < \varphi(t) < \hat{y}_r).$$

Proof. By hypothesis, we have that $m(y_2) < -\|f\|_\infty - a < \|f\|_\infty - a < m(y_l) = m(\hat{y}_l)$ (resp. $m(\hat{y}_r) < -\|f\|_\infty - a < \|f\|_\infty - a < m(y_1) = m(y_1)$), which implies that $\hat{y}_l$ (resp. y_1) is a lower solution and y_2 (resp. $\hat{y}_r$) is an upper solution. Then there is a T-periodic solution φ between $\hat{y}_l$, y_2 (resp. between y_1 and $\hat{y}_r$). □

Remark 2. In Fig. 4, we can notice that in $\{b \in \mathbb{R}^+ : b > b^*\} \times \mathbb{R}^+ - (A \cup B \cup C)$ the existence of at least one T-periodic solution cannot be guaranteed because the inequality (5) is not satisfied, for this reason the value T_l is introduced.

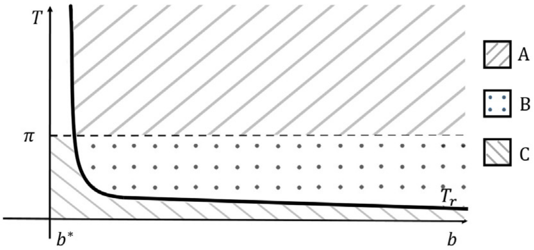

(a) Regions associated with Theorems 6 to 8.

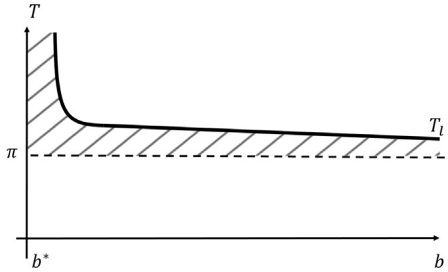

(b) Region associated with the Theorem 10.

Fig. 4. Regions on the plane b vs T where Eq. (2) has at least one T-periodic solution.

3.2. Multiplicity of periodic solutions

The conditions for the multiplicity of T-periodic solutions could be found for the case $b > b^*$ and in the same way as in the previous theorems, it is divided into the cases where $T < \pi$ and $T > \pi$. Moreover, as seen before, there is a relationship of existence with the values T_r and T_l, where multiplicity needs to be established.

In the proofs of Theorems 10 and 11, we used the fact that we can find a T-periodic solution between a well-ordered pair of lower and upper solutions as well as [29, Th. 1.15, Ch. III], which allowed us to find another solution, but it cannot be guaranteed that it is between a pair of lower and upper solutions.

For the following two theorems, we define the interval

$$I_7 = \Big]\, \|f\|_\infty - m(y_0), -m(y_l) - \|f\|_\infty \,\Big[\, .$$

Theorem 10. *If $b > b^*$, $T_r < T < \pi$ and $\|f\|_\infty < \dfrac{1}{2}|m(y_0) - m(y_l)|$, then (2) has at least three T-periodic solutions for $a \in I_7$.*

Proof. If $T_r < T < \pi$ we have that L has a unique solution y_0. By the hypothesis about a, we have $m(y_l) < -\|f\|_\infty - a < \|f\|_\infty - a < m(y_0)$, which implies that $r_a = y_0$ is an upper solution and $R_a = y_l$ is a lower solution. Therefore, there is at least one solution between y_0 and y_l. Since $T > T_r$, $m(\hat{y}_l) > m(y_0)$ thus y_r is an upper solution. Thus, there is another solution between y_l and y_r. To find the third solution, note that $\hat{y}_l$ is a lower solution since $m(\hat{y}_l) = m(y_l) < -a - \|f\|_\infty$. Hence, there is another solution between y_r and $\hat{y}_l$. □

Theorem 11. *If $b > b^*$, $T_r < \pi < T$ or $\pi < T_r < T$, and $\|f\|_\infty < \dfrac{1}{2}|(m(y_1) - m(y_l))|$, then (2) has at least three T-periodic solutions for $a \in I_7$.*

Proof. By the hypothesis on T, L has two solutions such that $y_1 < y_2$. Again, we have a solution between y_1 and y_l, and we can note that there exist a second solution between y_l and y_r in the same form as in the previous proof. To find the third solution, we must consider either $T < T_l$ or $T > T_l$.

When $T < T_l$, we have $y_2 > \hat{y}_l$, then a solution between y_r and $\hat{y}_l$ can be guaranteed.

When $T > T_l$, we have $y_2 < \hat{y}_l$ and we cannot guarantee that there is a solution between y_r and $\hat{y}_l$. To ensure the existence of such a solution, we use [29, Th. 1.15, Ch. III], then we can guarantee there is a t_1 such that the solution φ satisfies $\varphi(t_1) > y_r$. We must prove that every upper solution u with $u \geq y_r$ satisfies the condition $u < k$. Indeed, if $u \geq y_r$, then

$$u'' < m(u) + a + f(t) < m(y_r) + a + \|f\|_\infty .$$

Therefore, if u is a T-periodic solution, then there exists a $t_0 \in]0, T[$ such that $\min_{t\in]0,T[} u(t) = u(t_0) < \hat{y}_l$. Otherwise, $u'' < 0$ at t_0, which contradicts the periodicity of u. On the other hand, if u is extended periodically, $u'(t_0) = 0$, and for all $t \in]t_0, t_0 + T[$ we obtain

$$u(t) = u(t_0) + \int_{t_0}^{t} u''(s)(t-s)ds \leq y_s + (m(y_r) + a + \|f\|_\infty)\,\frac{T^2}{2}.$$

Thus, we find the third solution and we prove the theorem. □

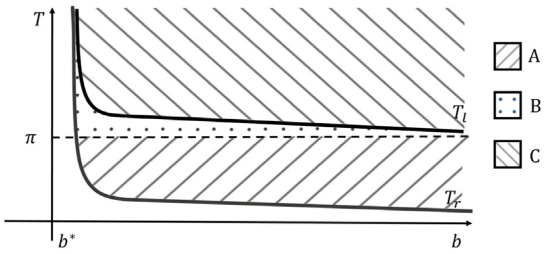

Fig. 5. Regions on the plane b vs T where Eq. (2) has at least three T-periodic solutions.

Table 1
Values for parameter involved in the T-periodic solutions of (2).

Parameter	Value
b^*	1.88988
b	2
y_r	1.47913
y_l	1.25992
$\hat{y}_r$	1.17815
$\hat{y}_l$	1.62806
T_r	5,07421
T_l	7,56147
y_1	1.01845

Corollary 1. *If $\|f\|_\infty < \frac{1}{2}(m(y_r) - m(y_l))$ and $a \in]\|f\|_\infty - m(y_r), -\|f\|_\infty - m(y_l)[$, then (2) has at least two T-periodic solutions.*

Remark 3. Fig. 5 shows the regions in the plane b vs T for which Theorems 10 and 11 guarantee there are at least three T-periodic solutions of Eq. (2). Note that the region C corresponds to conditions on T and b from Theorem 10 and that the two no well ordered solutions satisfy Proposition 2. On the other hand, the regions B and A are associated with Theorem 11, region B corresponds to the case in the proof where $T < T_l$ and A with the case $T > T_l$, furthermore one of the no well ordered solution does not have to satisfy Proposition 2.

4. Numerical results and discussion

In this section, we present numerical examples related to the main results in this work showing the presence of periodic oscillations which are associated to low and high amplitude solutions of the vibrating tip in an AFM. The parameter values of the AFM model can be found in [4]. For the purpose of our work, we assume that

$$f(t) = F\sin(\omega t), \quad F \in \mathbb{R},$$

where $w = \frac{2\pi}{T}$. The numerical values used for these examples can be seen in Table 1. On the other hand, to summarize our results we will use the Poincaré map, in this way we expect that the dynamics of Eq. (2) and, particularly, the T-periodic solutions could be observed.

For the existence of periodic solutions, we present the following example. Let be $T = \frac{\pi}{2}$, $\|f\|_\infty = 30$ and $a = 33 \in I_3$, such that Theorem 6 guarantee the existence of at least one solution between $y_1 = 1.01845$ and $R_a \approx 62$, as illustrated in the Poincaré map in Fig. 6. Note that the T-periodic solution corresponds to a point in the Poincaré map and this solution, in our case, is enclosed by quasiperiodic solutions that can be numerically restricted to estimate the T-periodic solution provided by Theorem 6.

It should be clarified that other numerical examples of existence can be done in the same way, by ensuring that the conditions of any of the Theorems 3 to 9 are met.

Now, for an example of multiplicity, let be $T = \frac{5}{2}\pi$, $\|f\|_\infty = 0.0012$ and $a = 2.3607 \in I_7$, then, we have that Theorem 11 guarantees the existence of at least three T-periodic solutions ϕ_1, ϕ_2 and ϕ_3 such that

$$1.01845 < \phi_1 < 1.25992 < \phi_2 < 1.47913 < \phi_3 < 1.62806.$$

Fig. 7 shows the Poincaré map where the T-periodic solution ϕ_1 is trapped on the left side of the figure, while the solution ϕ_3 is trapped on the right side. Similar to the previous example, these solutions are enclosed by quasiperiodic solutions. This behavior can also indicate that these solutions are stable. On the other hand, the solution ϕ_2 is between ϕ_1 and ϕ_3, and it is not enclosed by quasiperiodic solutions, which indicates that the solution is unstable and that finding it numerically will be more difficult. However, Theorem 11 gives us an estimate of where this solution should be.

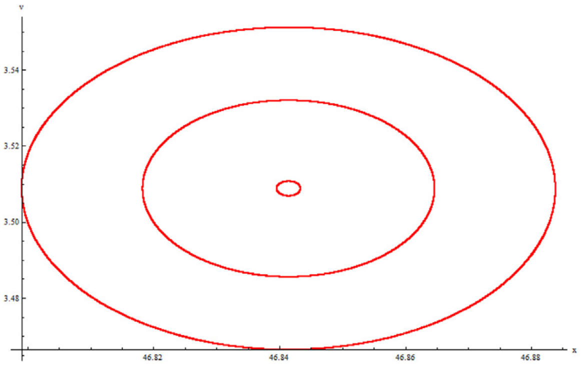

Fig. 6. Poincaré map for Eq. (2) taking the values of the Table 1 and $T = \frac{\pi}{2}$, $\|f\|_\infty = 30$ and $a = 33$.

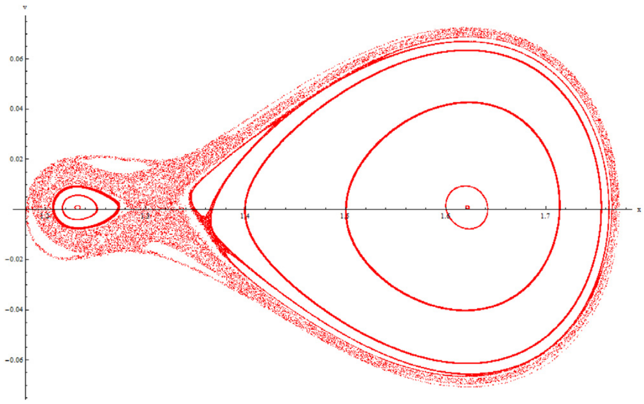

Fig. 7. Poincaré map of (2) taking the values from Table 1, $\omega = 1/T$, $T = \frac{5}{2}\pi$, $\|f\|_\infty = 0.0012$ and $a = 2.3607$.

For another interesting example, we take $T = 1$, $b = 30$ and $\|f\|_\infty = 10$, in such a way that we are under the conditions of Theorem 6. For these conditions we have that $y_1 = 0.708672$ and therefore $m(y_1) = -44.7245$. For the existence of at least one solution, it must be satisfied that $a > 54.7245$.

However, if we change the value of $a < 54.7245$, which is associated with the vertical distance between the tip and sample, the system present a strange behavior associated with an uncontrolled cantilever movement, and the system, could have strange behaviors as seen in Fig. 8, where the Poincaré maps are shown for different values of a between 1 and 20, with the initial condition at point $(1, 0)$. As can be seen, initially this "rabbit ears" figure appears, which gradually shows regions where subharmonics may exist and later a region in which there may be a set of quasiperiodic solutions where the periodic solution can be trapped, as in the above examples.

This latest behavior shows the instability of the system for changes in the parameters of the model, and in which chaotic behaviors have been verified in previous works based on the Melnikov method [16].

On the other hand, on Fig. 9 the initial condition has been changed to the point $(0.95, 0)$ and it can be seen that for the first values of a it is found a quasiperiodic solution where a T-periodic solution can be trapped. For this value, the presence of a periodic solution associated with a stable oscillation of the AFM is guaranteed and it verifies the case of parameter values for the stable oscillations. However, by moving a, the attractor set changes and then the "rabbit ears" appear.

5. Conclusion

Conditions for the existence and multiplicity of periodic solutions were established using the technique of upper and lower solutions for equations associated with a vibrating tip in an AFM with harmonic excitation. We found that there is an important change in the dynamics of the system when the parameters are modified, thus presenting points where there is a bifurcation. Numerical examples show how we can obtain the existence of one solution trapped in the upper and lower solution and similarly with at least three solutions, which is associated with stable oscillation of the low and high amplitude solutions of the AFM model. These results agree with the theoretical values of the AFM parameters related

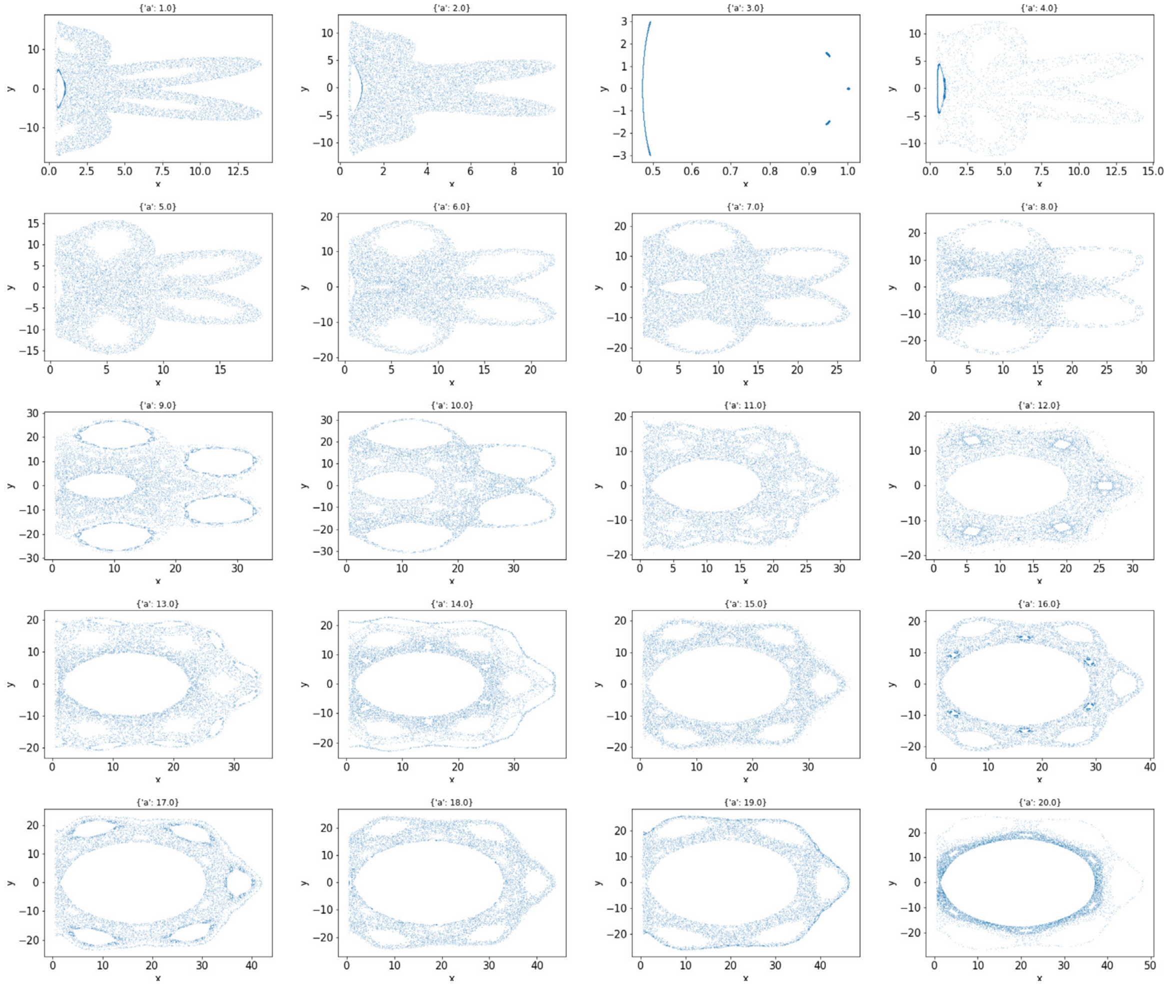

Fig. 8. Poincaré maps for $T = 1$, $b = 30$, $\|f\|_\infty = 10$ with initial condition $(1, 0)$ where the parameter a is taking values between 1 to 20.

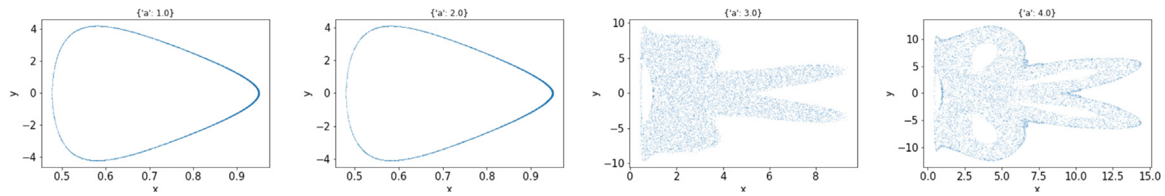

Fig. 9. Poincaré maps for $T = 1$, $b = 30$, $\|f\|_\infty = 10$ with initial condition $(0.95, 0)$ where the parameter a is taking values between 1 to 4.

to effective stiffness, tip–sample distance, and external excitation amplitude, which suggests that they are optimal to be implemented in the AFM systems design, for the topography imaging of different substances and materials in which the AFM techniques are widely used.

CRediT authorship contribution statement

Daniel Cortés: Conception and design of study, Acquisition of data, Analysis and/or interpretation of data, Writing – original draft, Writing – review & editing. **Alexander Gutierrez:** Conception and design of study, Acquisition of data, Analysis and/or interpretation of data, Writing – original draft, Writing – review & editing. **Johan Duque:** Acquisition of data, Analysis and/or interpretation of data, Writing – original draft.

Declaration of competing interest

The authors declare that they have no known competing financial interests or personal relationships that could have appeared to influence the work reported in this paper.

Acknowledgments

The authors are grateful to the referees for their useful suggestions which have helped us improve the quality of this paper. The authors D. Cortés and A. Gutiérrez have been financially supported by the Convocatoria Interna UTP 2020 (project CIE 3-21-5). All authors approved the version of the manuscript to be published.

References

[1] Binnig G, Quate CF, Gerber C. Atomic force microscope. Phys Rev Lett 1986;56(9):930–3.
[2] Deng J, Zhang L, Dong J, Cohen PH. Fm-based 3D nanofabrication using ultrasonic vibration assisted nanomachining. J Manuf Process 2016;24:195–202.
[3] Hail CU, Höller C, Matsuzaki K, et al. Nanoprinting organic molecules at the quantum level. Nature Commun 2019;10:1880. http://dx.doi.org/10.1038/s41467-019-09877-5.
[4] Younis MI. MEMS linear and nonlinear statics and dynamics. Springer; 2011.
[5] Morita S, Giessibl F, E. Meyer, et al. Noncontact atomic force microscopy. Springer; 2015.
[6] Garcia R, Pérez R. Dynamic atomic force microscopy methods. Surf Sci Rep 2002;47(6–8):197–301, September.
[7] Eslami S, Jalili N. A comprehensive modeling and vibration analysis of AFM microcantilevers subjected to nonlinear tip-sample interaction forces. Ultramicroscopy 2012;117:31–45, 2012.
[8] Bowen R, Hilal N. Atomic force microscopy in process engineering: introduction to afm for improved processes and products. Elsevier; 2009.
[9] Bhushan B, Marti O. Scanning probe microscopy-principle of operation, instrumentation, and probes. Springer Handb Nanotecnol 2004;1232.
[10] Chang WJ, Lee HL, Yang YC. Mathematical modeling of nanomachining with Atomic Force Microscope Cantilevers. J Phys Conf Ser 2014;490.
[11] Xu F, Guo X, Xu L, et al. Mechanical vibration measurement of solidly mounted resonator in fluid by atomic force microscopy. Micromachines 2017;8:244.
[12] Krull A, Hirsch P, Rother C, Schiffrin A. Artificial intelligence driven scanning probe microscopy. Commun Phys 2020;3:54.
[13] Hapala P, Švec M, Stetsovych O, et al. Mapping the electrostatic force field of single molecules from high-resolution scanning probe images. In: Nature communications, Vol. 7. 2016, p. 11560.
[14] Huang B, Li Z, Li J. Artificial intelligent atomic force microscope enabled by machine learning. Nanoscale 2018;45.
[15] Torres P. Mathematical models with singularities: a zoo of singular creatures. Atlantis Press; 2015, p. 124p.
[16] Ashhab M, Salapaka MV, Dahleh M, Mezic I. Melnikov-based dynamical analysis of microcantilevers in scanning probe microscopy. Nonlinear Dynam 1999;20:197–220.
[17] Brush SG. Interatomic forces and gas theory from Newton to lennard-jones. Arch Ration Mech Anal 1970;39(1):1–29.
[18] Jones JE. On the determination of molecular field. Proc R Soc Lond Ser A Math Phys Eng Sci 1924;106(738).
[19] Basso M, Giarre L, Dahleh M, Mezic I. Complex dynamics in a harmonically excited Lennard-Jones oscillator: Microcantilever-sample interaction in scanning probe microscopes. J Dyn Syst Meas Control 2000.
[20] Pai N, Wang C, Lin DT. Bifurcation analysis of a microcantilever in AFM system. J Franklin Inst 2010;347(7):1353–67.
[21] Jazi MM, Ghayour M, Ziaei-Rad S, E M. Miandoab effect of size on the dynamic behaviors of atomic force microscopes. Microsyst Technol 2018;24:1755.
[22] Zhang W, Meng G, Zhou J, Chen J. Nonlinear dynamics and chaos of microcantilever-based TM-AFMs with squeeze film damping effects. Sensors 2009.
[23] Gutierrez A, Cortés D, Castro DA. Saddle-node bifurcation and homoclinic persistence in AFM with periodic forcing. Math Probl Eng 2019;2019:6.
[24] Gutierrez A, Cortés D, Duque JS. Dynamics of a micro-electro-mechanical system associated with an AFM considering squeeze-film damping, Vol. 59 fasc. 13. Optical Society of America (OSA); 2020, p. 76–80.
[25] Zhang T, Xiong L. Periodic motion for impulsive fractional functional differential equations with piecewise Caputo derivative. Appl Math Lett 2020;101.
[26] Zhang T, Zhou J, Liao Y. Exponentially stable periodic oscillation and Mittag–Leffler stabilization for fractional-order impulsive control neural networks with piecewise Caputo derivatives. IEEE Trans Cybern 2021;2168–267.
[27] Magnus W, Winkler S. Hill's equation. Dover Publications; 2013.
[28] Torres P. Existence and uniqueness of elliptic periodic solutions of the Brillouin electron beam focusing system. Math Methods Appl Sci 2000;23:1139–43.
[29] De Coster C, Habets P. Two-point boundary value problems: lower and upper solutions, mathematics in science and engineering. Elsevier; 2006.
[30] Lazer AC, Solimini S. On periodic solutions of nonlinear differential equations with singularities. Proc Amer Math Soc 1987;99:109–14.
[31] Lynch S. Dynamical systems with applications using python. Springer; 2018.